Signal-piloted processing metaheuristic optimization and wavelet decomposition based elucidation of arrhythmia for mobile healthcare

Signal-Piloted Processing Metaheuristic Optimization and Wavelet Decomposition based Elucidation of Arrhythmia for Mobile Healthcare

Article *in* Biocybernetics and Biomedical Engineering · May 2022

DOI: 10.1016/j.bbe.2022.05.006

CITATIONS
2

READS
142

5 authors, including:

Saeed Mian Qaisar
Effat University
202 PUBLICATIONS **1,246** CITATIONS
SEE PROFILE

Sibghatullah Inayatullah Khan
Sreenidhi Institute of Science & Technology
26 PUBLICATIONS **73** CITATIONS
SEE PROFILE

Dominique Dallet
Bordeaux INP
331 PUBLICATIONS **1,988** CITATIONS
SEE PROFILE

Ryszard Tadeusiewicz
AGH University of Science and Technology in Kraków
443 PUBLICATIONS **3,179** CITATIONS
SEE PROFILE

Signal-Piloted Processing Metaheuristic Optimization and Wavelet Decomposition based Elucidation of Arrhythmia for Mobile Healthcare

Saeed Mian Qaisar[1,*], Sibgatullah I. Khan[2], Dominique Dallet[3], Ryszard Tadeusiewicz[4], Paweł Pławiak[5,6,*],

[1] Dept. of Electrical and Computer Engineering, Effat University, 22332, Jeddah, KSA. [ORCID ID: https://orcid.org/0000-0002-4268-3482].
[2]Electronics and Communication Department, Sreenidhi Institute of Science and Technology, Hyderabad, India.
[3]University of Bordeaux, CNRS, Bordeaux INP, IMS, UMR 5218, 33400 Talence, France.
[4]AGH University of Science and Technology, Department of Biocybernetics and Biomedical Engineering, Krakow, Poland
[5]Department of Computer Science, Faculty of Computer Science and Telecommunications, Cracow University, of Technology, Warszawska 24, 31-155 Krakow, Poland
[6]Institute of Theoretical and Applied Informatics, Polish Academy of Sciences, Baltycka 5, 44-100 Gliwice, Poland.

* Corresponding Authors: Paweł Pławiak (plawiak@pk.edu.pl) and Saeed Mian Qaisar (sqaisar@effatuniversity.edu.sa)

Abstract —The next generation healthcare systems will be based on the cloud connected wireless biomedical wearables. The key performance indicators of such systems are the compression, computational efficiency, transmission and power effectiveness with precision. The electrocardiogram (ECG) signals processing based novel technique is presented for the diagnosis of arrhythmia. It employs a novel mix of the Level-Crossing Sampling (LCS), Enhanced Activity Selection (EAS) based QRS complex selection, multirate processing, Wavelet Decomposition (WD), Metaheuristic Optimization (MO), and machine learning. The MIT-BIH dataset is used for experimentation. Dataset contains 5 classes namely, “Atrial premature contraction”, “premature ventricular contraction”, “right bundle branch block”, “left bundle branch block” and “normal sinus”. For each class, 450 cardiac pulses are collected from 3 different subjects. The performance of Marine Predators Algorithm (MPA) and Artificial Butterfly Optimization Algorithm (ABOA) is investigated for features selection. The selected features sets are passed to classifiers that use machine learning for an automated diagnosis. The performance is tested by using multiple evaluation metrics while following the 10-fold cross validation (10-CV). The LCS and EAS results in a 4.04-times diminishing in the average count of collected samples. The multirate processing lead to a more than 7-times computational effectiveness over the conventional fix-rate counterparts. The respective dimension reduction ratios and classification accuracies, for the MPA and ABOA algorithms, are 29.59-times & 22.19-times and 98.38% & 98.86%.

Keywords: Arrhythmia classification; Compression; Dimension reduction; Electrocardiogram (ECG); Feature Extraction; Healthcare, Level-crossing sampling; Multirate processing; Metaheuristic optimization; Machine Learning; QRS selection, Wavelet decomposition.

1. Introduction

1.1 Background and Related Works

The rising frequency and incidence of cardiovascular illnesses has garnered the attention of the “World Health Organization” (WHO) [1]. As per WHO, on average 17.9 million lives are globally lost due to this disease.

The fatality rate from cardiovascular disorders has decreased as a result of recent developments in medicine, monitoring, and diagnosis [1]. The Electrocardiogram (ECG) can be utilized to perform a non-invasive heart function examination. The heart's functioning can be disrupted, resulting in abnormal patterns known as "cardiac arrhythmia." Arrhythmias can be identified effectively if the ECG signals are properly analysed [1]. An accurate and timely diagnosis can save lives.

In fact, manually analyzing the ECG is time-consuming and laborious. It is particularly challenging in the case of big datasets and can lead towards a wrong diagnosis. This difficulty can be handled by employing a computer-assisted automated ECG signals analysis [2]. It permits the detection of minor variations in the frequency and amplitude content of cardiac pulses. Therefore, it is possible to augment the identification of different arrhythmias [3].

The first processing step, in the computer-assisted diagnosis of heart diseases, is preconditioning. It prevents the unwanted noise from the incoming signal and prepares it for a successful extraction of features. Certain studies also consider the QRS complex selection during preconditioning [4], [5], [6]. The known noise removal approaches include “digital filtering”, “Principle Component Analysis” (PCA), “Wavelet Transform" (WT), and “Kalman Filtering” [2], [3]. The next and crucial step is the extraction of features. Some known feature extraction methods are the "Discrete Cosine Transform" (DCT), "Short Time Fourier Transform" (STFT), “empirical Mode Decomposition” (EMD) and "Discrete Wavelet Transform" (DWT). The mined features are afterward conveyed to the classifier. Some known arrhythmia classifiers are the "K-Nearest Neighbor" (KNN), "Artificial Neural Networks" (ANN), "Support Vector

Machine" (SVM), and “Random Forest” (RF).

The QRS complexes are extremely significant parts of the ECG signal. They play a vital role in the detection of heart disorders [4]. In [4], authors had presented an embedded algorithm for recognizing the QRS complexes. The shape, slope, and time duration among suggestive QRS complexes were used for their recognition. The DWT was used in [5] to recognize the QRS complexes of an ECG signal. For the identification of QRS complexes, an empirical comb derivative filter was used in [6]. In [4], [5] and [6] the system performance was measured in terms of the QRS detection precision.

In recent years, several ECG based methods have been presented for an automated arrhythmia diagnosis [3], [7], [8], [9], [10], [11], [12], [13], [14], [15], [16], [17], [18]. In [3], Sandeep and Kailash had used the DCT based Discrete Orthogonal Stockwell Transform (DOST) for feature extraction. The dimension reduction was performed with PCA. The output of PCA was combined with morphological features and R-R interval to prepare the classifiable features set. The recognition of arrhythmia was performed by using the SVM algorithm. In [8], Qaisar and Dallet had carried out the feature extraction by using the WD. The subband coefficients ware conveyed to the ANN classifier for an automated categorisation of arrhythmias. In [17], Qaisar et al. had extracted statistical features from subbands, obtained by using the DWT. The features selection was carried out with the Mutual Information (MI) approach. Onward, the retained features were classified by the RF algorithm. In [19], the DWT based subbands statistical features were extracted. The RF classifier was used for categorization.

In recent years, the arrhythmia identification is also performed by using the deep learning methods. Hammad et al., [7], used Long-Short-Term-Memory (LSTM) based Deep Learning Model (DLM) for feature extraction. The Genetic Algorithm (GA) was used for dimension reduction and classification was carried out with Deep Neural Network (DNN). Sahoo et al., [9], employed DWT in conjunction with temporal and morphological methods to extract features. The classification was performed by using the SVM. In [10], Yildirim et al. used a nonlinear encoding structure based on a convolutional auto-encoder with LSTM classifiers to automatically identify arrhythmias. Atal et al., [11], retrieved wave and Gabor features and classified them by using a Convolutional Neural Network (CNN). In [12], authors had used a Deep CNN (DCNN) model to process the conditioned ECG signals for arrhythmia identification. Huang et al., [13], used the ECG spectrogram along with a 2-D CNN for the categorization of arrhythmias. In [14], authors used denoising auto encoders for feature extraction and a DNN for the classification. In [15], a mix of CNN and LSTM was used to process the conditioned ECG signals for arrhythmia classification. In [16], CNN was used for the classification of conditioned ECG signals in the context of arrhythmia diagnosis. In [18], feature extraction was performed by using the LSTM based autoencoder and the classification was carried out by using the SVM algorithm.

1.2 Motivation and Contribution

The immediate treatment is not necessary for mild a rrhythmias. However, in critical situation alternative opt ions such as the cardiac defibrillation or surgery can b e considered. Therefore, patients with crucial condition require uninterrupted monitoring. The wearable and wire less ECG sensors are beneficial in this situation [20], [21], [22], [23], [24], [25]. These are typically connected to the cloud via IoMT for further processing [19], [25]. It is critical to keep track of the multi-channel ECG signals in order to make an appropriate diagnosis [26]. However, this generates a huge amount of data to manage and analyse [27]. A viable implementation necessitates processing and power efficiencies [20], [28]. In this scenario, the compression [21], random sampling [29], compressive sensing [27], [30], [31], multirate processing [8], [17], and metaheuristic optimization (MO) based dimension reduction techniques [32], [33] have been investigated. It has been shown that a substantial saving of memory, power and transmission activity can be reached by diminishing the activity of acquisition, processing, and wireless data transmission [22], [23], [24], [25].

Most of the existing ECG systems are based on the fix-rate uniform sampling concept [3], [7]-[10], [11]-[18]. Consequently, the system can gather and analyzes unneeded data in the case of ECG like sporadic signals. It burdens by rising the computing load, transmission activity and power consumption [34]. It is particularly not best suited for the mobile healthcare systems.

The solutions presented in [4], [5], [6], [21], [27], [30] and [31] achieve compression and sparse representation by processing the uniformly acquired ECG signals. This is not the best practice for wireless gadgets with stringent constraints.

In this context this study brings an original solution to the above raised concerns. It uses the signal-piloted level-crossing sampling based data acquisition [8], [19], [23], [25]. This induces the compression by diminishing the activity of data acquisition. Therefore, the application of post-acquisition compression and decompression algorithms is avoided. Additionally, the computational effectiveness of the system can be enhanced by adjusting the parameters of online signal processing stages in accordance with the incoming signal variations [34].

The level-crossing based QRS detection approaches have been presented in [23], [25] and [35]. However, the complete automated arrhythmia classification solutions based on the level-crossing sampling and machine learning were first time presented by Qaisar et al. in [8] and [19]. Building upon these works, a new method is proposed with an improved arrhythmia identification precision. The major contribution is:

- Proposing an original hybridization of ECG adaptive-rate acquisition, Enhanced Activity Selection (EAS) based QRS selection, multirate processing, WD, subbands selection, MO based dimension reduction, and machine learning for an effective elucidation of arrhythmia:

1). The ECG signals are captured at adaptive-rates, piloted by signal, by using the level-crossing analog to digital converters (LCADCs). The EASA is used for the QRS

complexes selection.

2). The denoising is accomplished with a lower-tap filter. The decimation is incorporated before WD. The decimated segments are decomposed in subbands by using the suggested WD scheme. The subbands are selected on the basis of frequency content.

3). To dimension reduction is attained by using the MO based algorithms. The performance of MPA and ABOA is studied and compared in terms of dimension reduction and identification accuracy. The machine learning based classifiers are used for processing the extracted features sets.

To the best of the authors' knowledge, it is the first attempt to achieve an automated identification of arrhythmia in the above enumerated manner. The findings are promising in terms of reducing the data dimension and computational complexity of the system while maintaining a high arrhythmia detection accuracy, sensitivity, specificity, F1-Score, Kappa statistics, and area under the Receiver Operating Characteristics (ROC) curve (AUC).

1.3 Paper Outline

The rest of paper is organized as follows. Section 2 covers details of the suggested approach and dataset, used through the execution and validation process. In Section 3 the findings are presented. Section 4 contains the performance analysis and discussion of the outcomes. Section 5 draws conclusion.

2. Materials and Methods

The overall design of our arrhythmia classification system is shown in Fig. 1. Where, MOFS stands for the MO based features selection (FS). The features sets P_R, P_T, and P_b are described in Section 2.1.

The ECG wearable processing stages are encased in the dotted, blue-color border ('….'). The resampling, conditioning, decimation, WD, FS, and classification are suggested to be implemented on the cloud server. The benefit of this strategy is a reduction in the data transfer. It is beneficial for wireless cloud connected wearable devices in the context of mobile healthcare. This strategy enables the development of biomedical implants which are tailored for a specific application while preserving the signal processing and classification algorithms easily updateable.

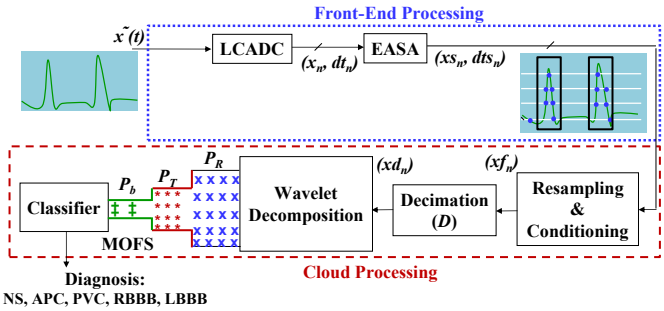

Fig.1. The proposed system block diagram.

[1] ECG arrhythmia time series are available under (https://physionet.org/content/mitdb/1.0.0/

2.1 Dataset

To examine the system performance, the MIT-BIH dataset[1] is used [36]. The ECG signals are band limited with analog low-pass filter with a cutoff frequency of 60Hz. Onward, each band limited channel is captured by using a 11-Bit resolution ADC that operates at a sampling frequency of 360Hz. The ECG recordings are analyzed and categorized by experienced cardiologists.

According to the statistics of dataset [36], for various arrhythmia, the average cardiac pulse duration is limited to 0.9-second. Therefore, the individual heartbeats are extracted from the intended records by using 0.9-second fixed length windows, centered on R-peaks, for the classical case. The information about R-peaks is retrieved from the dataset [36]. In the suggested approach, this segmentation is achieved by using the EASA based QRS complexes selection, applied on multiple 30-second long ECG signals (cf. Section 2.3). Each obtained segment is called an instance. "Atrial premature contraction" (APC), "premature ventricular contraction" (PVC), "right bundle branch block" (RBBB), "left bundle branch block" (LBBB) and "normal sinus" (NS) are the five clinically important types of arrhythmias which are investigated. To avoid any prejudice, each intended arrhythmia class is given an equal representation. A total of 450 instances are considered for each class. This results in a total of 2250 instances across the five categories. To prevent any bias, heartbeats for each category are gathered from three different recordings/subjects (cf. Fig.2).

The WD scheme is employed for decomposing each ECG instance (cf. Section 2.5). To demonstrate the performance of used subbands selection and MO based dimension reduction methods, the classification performance is studied for different features sets P_R, P_T and P_b:

The P_R is created by concatenating coefficients from all obtained subbands. Onward, the P_T is created by extracting coefficients from the selected subbands. This selection is made on the basis of frequency content. Afterward, the MPA and ABOA based features are selected from P_T. It generates P_b, where, $b \in \{1, 2\}$ and is indexing the features set generated respectively with the MPA and ABOA.

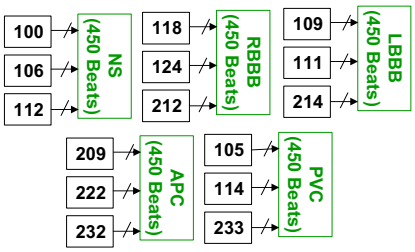

Fig.2. The arrhythmia records used to extract ECG beats in this study.

2.2 Level-Crossing ADC (LCADC)

Let $\boldsymbol{y(t_n)}$ be the band-limited sampled signal, retrieved from the considered dataset. Then it is reconstructed and used to test the LCADC. The process is given as: $\tilde{\boldsymbol{x}}(\boldsymbol{t}) = \boldsymbol{y}(\frac{\boldsymbol{t_n}}{\boldsymbol{U}})$. The cascaded spline interpolator is used for reconstruction [37]. $\tilde{\boldsymbol{x}}(\boldsymbol{t})$ is the analog like version of $\boldsymbol{y(t_n)}$ and $\boldsymbol{U}$=200 is the factor of up-sampling.

In this study, the LCADC contains a 5-bit digital-to-analog converter (DAC), a 5-Bit up/down binary counter, a timer and a difference quantifier with hysteresis [38]. The LCADC's dynamic range, ΔV =±1mV, and resolution, M=4.4-Bit, are both known. They set the quantization step as $q = \frac{\Delta V}{2^M}$. For the chosen value of M, the LCADC has 21 uniformly spaced thresholds. An incremental approach is adopted, to choose the number of LCADC thresholds, while attaining a favorable compromise between the complexity and precision. The functioning steps of LCADC are described in [38]. It generates amplitude-time pair, (x_n, dt_n), for the n^{th} sample. Here x_n is the amplitude of n^{th} sample and dt_n is the interval between the n^{th} and the $(n\text{-}1)^{th}$ sampling instances.

The used LCADCs are based on a different governing theory than conventional ADCs [38]. In contrast to the conventional ADCs, their Signal to Noise Ratio (SNR) is independent of M and it depends on the F_{Timer} [38]. For an ideal LCADC, the SNR is given by Eq. (1). Where f_{sig} is the frequency of full-scale sinusoid and $T_{Timer} = \frac{1}{F_{Timer}}$ [38].

The amplitude of $\tilde{x}(t)$ is scaled to make $\Delta\tilde{x}(t) = \Delta V$. It ensures that each considered arrhythmia category shares a common scale. The value of T_{Timer} is selected by using the tracking condition: $\left|\frac{d\tilde{x}(t)}{dt}\right| \leq \frac{q}{T_{Timer}}$. Here, $\left|\frac{d\tilde{x}(t)}{dt}\right| \leq 2\pi \times \Delta\tilde{x}(t) \times f_{max}$ [38]. f_{max} is the bandwidth of $\tilde{x}(t)$. A proper value of T_{Timer} can be selected as $T_{Timer} \leq \frac{1}{2\pi \times f_{max} \times 2^M}$ [38]. In this study, T_{Timer} =125µSeconds is selected with 13-Bit timer resolution. It allows a heartbeat to be captured without the timer overflow.

$$SNR_{dB} = -5.17 - 20log\left(f_{sig}.T_{timer}\right). \quad (1)$$

The process of conducting the QRS based segmentation, on the LCADC outcome, is presented in Section 2.3.

2.3 The Enhanced Activity Selection Algorithm (EASA)

The EASA is based on the concept of non-uniformity in the level-crossing sampling. It employs the idea, presented by Qaisar et al. in [35], to segment the QRS complexes. The functioning steps are described in the following.

Step I: Let the i^{th} selected segment, W^i, has N^i samples and L^i length (in Seconds). The L^i and N^i are set to zero in the start of each iteration.

Step II: We keep adding samples in W^i till $L^i \leq L_{ref}$ and $dt_n < T_0$. L_{ref} is the upper bound on L^i and T_0=200mSec is used as a threshold of signal activity detection [34], [35]. For an added sample, the new L^i and N^i are computed as $L^i = L^i + dt_n$ and $N^i = N^i + 1$.

Step III: Once $L^i > L_{ref}$ or $dt_n > T_0$, the next iteration is started.

Step IV: The condition $N^i \geq N_{ref}$ verifies the validity of W^i. Here, N_{ref} is the reference number of samples.

A QRS complex is supposed to exist in each validated W^i. L_{ref}=500mSec and N_{ref}=50 are chosen in this study. This choice is made while considering widths and amplitudes disparities of the QRS complexes in the intended dataset [36].

The processes of conditioning and decimating the instances, obtained with EASA, are described in Section 2.4.

2.4 The Resampling Conditioning and Decimation

The W^i can be further processed by using the high complexity non-uniform filtering tactics [34]. However, to attain an efficient noise removal, the W^i is resampled uniformly. This permits the incorporation of mature classical filtering algorithms. After resampling, there exists N_r^i samples in W^i.

The Simplified linear interpolation (SLI) is used to perform the online resampling [39]. Properties of the resampled signal can be different compared to the original one. In [39], it is shown that for SLI the error per resampled point is confined by $\frac{q}{2}$.

The useful spectrum of the ECG signals, for arrhythmia identification, is between [0; 22] Hz [40]. Therefore, a low-pass 58th order FIR filter with the cut-off frequency, F_C =35Hz, and $Fref$ =180Hz sampling frequency is implemented offline by using the Parks–McClellan algorithm. The process is mathematically given by Eq. (18). This filtering operation with post decimation and used WD allows focusing on the intended band of interest.

The sampling frequency of each W^i can be specific and is given as: $Fs^i = \frac{N^i}{L^i}$ [34]. To achieve a proper online filtering the W^i should be resampled at $Fref$ [34]. The filtered signal, xf_n, is onward decimated with a factor of $D = 2$ to obtain $xd_n = xf_{Dn}$. The choice of $D = 2$, for the studied case, adheres to the condition: $D \leq \frac{180}{F_{Nyq}} = 2.57$ and, thus, does not induce aliasing [17]. Here, $F_{Nyq} = 2.f_{maxf}$ and f_{maxf}=35Hz is the bandwidth of xf_n. The decimation further reduces the computational complexity by lowering the quantity of data to be processed by the following stages.

Each decimated instance, xd_n, is decomposed by using the proposed WD scheme (cf. Section 2.5).

2.5 The Wavelet Decomposition (WD)

The mathematical representation of wavelets is given by Eq. (2). Where, the translation and dilation parameters are presented by z and v respectively [2]. The process of decomposing a signal, $y(t)$, with wavelet transform is given by Eq. (3).

$$\Psi(t) = \frac{1}{\sqrt{v}}\psi((t-z)/v) \quad (2)$$

$$W_x(u,s) = \frac{1}{\sqrt{v}}\int_{-\infty}^{+\infty} x(t)\psi^*((t-z)/v)\,dt \quad (3)$$

The "Wavelet Decomposition" (WD) is used for decomposing the decimated signal xd_n. In [2], [9] and [41], the effectiveness of Daubechies wavelets is shown for arrhythmia categorisation. Therefore, the xd_n is splitted in subbands by using the Daubechies, db4, wavelets. The half-band digital filters deliver the "approximation", a_m and "detail", d_m, coefficients. The procedure is shown in Fig. 3 and also given by Eq. (4) and Eq. (5).

$$a_m = \sum_{k=1}^{K_q} xd_n \cdot g_{2n-k}. \quad (4)$$

$$d_m = \sum_{k=1}^{K_q} xd_n \cdot h_{2n-k}. \quad (5)$$

Where, the half-band low-pass and high-pass filters, of length Q+1, are g_{2n-k} and h_{2n-k} respectively. m is the count of decomposition stages and is: $m \in \{1, 2, 3, 4\}$.

The subband coefficients dd4, da4, ad4 and aa4 are selected. It permits to focus on the frequency band of interest. There are 9 coefficients in each selected subband. Hence, each instance is represented by the 36 features. Coefficients of all subbands (d1, d2, dd4, da4, ad4 and aa4) are included in the first features set, P_R. It yields 78 features per instance and generates P_R = 2250×78. The second features set, P_T, contains coefficients from selected subbands (dd4, da4, ad4, and aa4). It generates P_T = 2250×36.

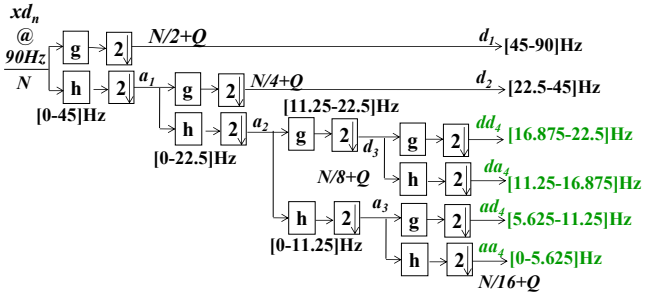

Fig.3. The used wavelet decomposition scheme.

Features from P_T are further selected by using the considered MOFS approaches as described in Section 2.6.

2.6 Metaheuristic Optimization (MO) based Features Selection

The FS task is important as it aids in reducing the system complexity and improves its dimension reduction [17]. In current study, for both considered MO algorithms, the maximum numbers of iterations are fixed to 100.

a) **Marine Predators Algorithm (MPA):** The MPA is inspired from the foraging and hunting behavior of marine predators (MP) and prey [42]. In MPA, the MP and prey are considered as potential solutions. The initial population (X_0) of MP and prey is defined randomly by Eq. (6) [42].

$$X_0 = Lb + r(Ub - Lb) \ . \quad (6)$$

where, *Lb* and *Ub* denote the lower and upper bound of variables, and *r* is a random number in the range of [0,1] [42]. From the initial random solutions, the best solutions are placed in the matrix, which is called as *Elite (E)* [42].

The MPA operates in three phases. Each phase consists one third of total iterations. In the first phase, the velocity parameter is high $(v > 10)$ and the prey moves faster than MP. In the first phase, the prey follows Lévy motion. The movement in the first phase is described by Eq. (7) [42].

$$\overrightarrow{STPsize_i} = \vec{R}_B \otimes (E_i - \vec{R}_B \otimes \overrightarrow{Prey_i}) \quad i = 1, \ldots n$$
$$\overrightarrow{Prey_i} = \overrightarrow{Prey_i} + P.\vec{R} \otimes STPsize_i. \quad (7)$$

The $\overrightarrow{STPsize}$ denotes the step size of i^{th} solution. The vector $\vec{R}_B$ contains the random numbers defined from the normal Brownian distribution. The symbol $\otimes$ denotes entry wise multiplication. The *P* is constant and is fixed at 0.5, and the *R* denotes the random number between [0,1][42].

In the second phase, the velocity of MPs and prey is same. The velocity value in this phase is unity, with the Preys follows the Levy motion and MPs follow the Brownian motion. The movements in the second phase (for next one third of maximum iterations) are described by Eq. (8) [42].

$$\overrightarrow{STPsize_i} = \overrightarrow{R_L} \otimes \left(\overrightarrow{E_i} - \overrightarrow{R_L} \otimes \overrightarrow{Prey_i}\right) \quad i = 1, \ldots \frac{n}{2}$$
$$\overrightarrow{Prey_i} = \overrightarrow{Prey_i} + P.\vec{R} \otimes \overrightarrow{STPsize_i}. \quad (8)$$

The $\overrightarrow{R_L}$ denotes the vector which consists of random numbers corresponding to the Levy distribution. The Levy movement of Prey is represented by the product of $\overrightarrow{R_L}$ and $\overrightarrow{Prey}$. As mentioned earlier, only 50% of the population is engaged in the exploitation, the remaining 50% population is responsible for exploration as given by Eq. (9) [42].

$$\overrightarrow{STPsize_i} = \overrightarrow{R_B} \otimes \left(\overrightarrow{R_B} \otimes \overrightarrow{E_i} - \overrightarrow{Prey_i}\right) \quad i = 1, \ldots \frac{n}{2}$$
$$\overrightarrow{Prey_i} = \overrightarrow{E_i} + P.CP \otimes \overrightarrow{STPsize_i}. \quad (9)$$

The parameter CP denotes the control parameter, which controls the step size of MP and it is given by Eq. (10) [42].

$$CP = \left(1 - \frac{C_{iter}}{M_{iter}}\right)^{2\left(\frac{C_{iter}}{M_{iter}}\right)}. \quad (10)$$

Where, the current and maximum number of iteration is denoted by C_{iter} and M_{iter}, respectively. The movement of MP is represented by the product of $\overrightarrow{R_B}$ and $\overrightarrow{E_i}$.

In phase 3, the MP moves faster than Prey. This phase corresponds to the exploitation phase of MPA. The velocity in this phase is low ($v = 0.1$). In this phase the MP follows the Levy motion. The movement in this phase is represented by Eq. (11) [42],

$$\overrightarrow{STPsize_i} = \overrightarrow{R_L} \otimes \left(\overrightarrow{R_L} \otimes \overrightarrow{E_i} - \overrightarrow{Prey_i}\right) \quad i = 1, \ldots n$$
$$\overrightarrow{Prey_i} = \overrightarrow{E_i} + P.CP \otimes \overrightarrow{STPsize_i}. \quad (11)$$

The Levy movement of the MP is represented by the product of $\overrightarrow{R_L}$ and $\overrightarrow{E_i}$. The addition of step size to $\overrightarrow{E_i}$

position represents the MP movement, which aid in update in the Prey position. This phase runs from two third of maximum iteration to maximum number of iterations.

b) **Artificial Butterfly Optimization Algorithm (ABOA):** The ABOA is inspired from the mate finding strategy of a woodland butterfly known as speckled wood [43]. In ABOA the first step is to initialize and evaluate the fitness of each butterfly. Depending on the fitness, the butterflies are sorted into sunspot and canopy group. The sunspot and canopy butterflies follow the flight mode to update their locations as given by Eq. (12) [43].

$$X_{i,j}^{t+1} = X_{i,j}^{t} + \left(X_{i,j}^{t} - X_{k,j}^{t}\right).rand(). \quad (12)$$

In the above equation, the $X_{i,j}^{t}$ and $X_{i,j}^{t+1}$ respectively denote the i^{th} butterfly at t and $t+1$ iteration in the j^{th} dimensional search space. $X_{k,j}^{t}$ is the k^{th} butterfly ($i \neq k$), and $rand()$ is randomly generated number between -1 and +1. The updated butterflies are now evaluated for fitness, and sorted according to the greedy selection.

In the next phase, the butterflies fly in the free flight mode can be given by Eq. (13) [43].

$$X_{i,j}^{t+1} = X_{i,j}^{t} + \frac{X_{k,j}^{t} - X_{i,j}^{t}}{\left\|X_{k,j}^{t} - X_{i,j}^{t}\right\|}(U - L)s.rand(). \quad (13)$$

In the above equation, the quantity $\left\|X_{k,j}^{t} - X_{i,j}^{t}\right\|$ represents the distance between the $X_{k,j}^{t}$ and $X_{i,j}^{t}$ butterflies. The upper and lower bounds of search space are respectively denoted by U and L. The step size is s, which decreases with the increase in iteration, i.e., it controls the exploration and exploitation as given by Eq. (14) [43].

$$s = 1 - (1 - s_e)\left(\frac{T_c}{T_{\max}}\right). \quad (14)$$

where, s_e is the control parameter fixed at 0.02 [43]. The T_c denotes current iteration and $T_{\max}$ denotes maximum number of iterations. During the free flight phase, the butterflies fly in the random fashion, and this phase represents the exploration in ABOA. The Eq. (15) governs the free flight mode of ABOA [43]:

$$X_{i,j}^{t+1} = X_{k,j}^{t} - 2\alpha.rand() - \alpha D. \quad (15)$$

The parameter α decreases linearly from 2 to 0 during the entire iterations [43]. The parameter D is obtained by using Eq. (16) [43] as,

$$D = \left|2.rand()\left(X_{k,j}^{t} - X_{i,j}^{t}\right)\right|. \quad (16)$$

2.7 Classification Methods

To categorize the feature sets (P_R, P_T, P_1 and P_2) in this work, four distinct classifiers are used: ANN, SVM, KNN, and RF.

In this study four different classifiers namely, ANN, SVM, KNN, and RF are used to classify the features sets, P_R, P_T, P_1 and P_2. They were chosen from a list of commonly used arrhythmia classification methods in the literature. The hyperparameter tuning processes are studied to identify the optimal settings for each classification technique. To standardize the range of features, a min-max scalar is employed between [0, 1], before classification. For each class, a multi-subject dataset with 10-CV and numerous assessment matrices such as "accuracy", "specificity", "sensitivity", "F-measure", "Kappa", and Area Under the "Receiver Operating Characteristics" (ROC) curve (AUC) is utilized to prevent bias and overfitting.

a) **Artificial Neural Network (ANN):** The ANN is built using the notion of biological neural networks [44]. An artificial neuron is the fundamental component of an ANN. The three basic operations, performed by an ANN, are multiplication, summation, and activation. As a result, an ANN is made up of a collection of connected input and output units. Learning is accomplished by updating the weights of each link, resulting in the classification of test data. In this research, the multilayer perceptron (MLP) architecture is used. The optimal topology is attained by employing five hidden layers.

b) **K-Nearest Neighbor (k-NN):** The k-NN searches for k samples that are the most similar to the predicted one. Each neighbor is given the opportunity to vote. The most popular class is allocated to the predicted sample [44]. The choice is depending on the distance measure. Different values of k are evaluated one by one until the k=5 value with the lowest classification error is chosen.

c) **Support Vector Machine (SVM):** The SVM [44] is a widely used supervised learning approach that tries to optimize the distance between two classes by building a hyperplane between them. A polynomial of degree=3 is utilized in this study, and the cost parameter C is set at 100 [44].

d) **Random Forest (RF):** The RF is a classification method that use ensemble learning to improve results by building several Decision Trees (DTs). The precision of the categorization is related to the accuracy of the tree [44]. The optimal number of estimators for the random forest in our method is 100.

2.8 Performance Evaluation Measures

a) **Size Reduction Ratio (SRR):** The SRR is given by Eq. (17). Where, N and N_P are the count of samples collected and transmitted, towards cloud, respectively in the traditional and suggested approaches.

$$SRR = \frac{N \times Number\ of\ Bits\ per\ Sample}{N_P \times Number\ of\ Bits\ per\ Sample}. \quad (17)$$

b) **Computational Complexity:** It makes a comparison of the devised method and fixed-rate alternatives in terms of the

number of fundamental operations like multiplications and additions that must be performed [45]. The complexity is examined in detail for all adaptive-rate processing stages till the WD, while the classification module is a standard one.

The processing principle for the fixed-rate counterparts is depicted in Fig. 4. In this case, the processing is carried out at a fix-rate of 360Hz [36]. x_n is windowed in cardiac pulses, each with a length of 0.9-Seconds and N_r=324 samples. This segmentation is carried out with a rectangular window function, centered on R-peaks, and it has a negligible processing cost [37]. Following that, each segment is conditioned by using a FIR filter. This filter operates at $F_S = 360$Hz and is developed with the same settings as in Section 2.4. It renders a 117th order filter. When computing a filtered outcome, the computational cost of a K_F -order FIR filter is $K_F - 1$ additions and K_F multiplications. Consequently, the complexity of denoising N_F samples can be expressed by Eq. (18).

$$C_{Classic-FIR} = \underbrace{(K_F - 1) \times N_F}_{Additions} + \underbrace{K_F \times N_F}_{Multiplications} . \quad (18)$$

Onward the signal is decomposed by using the similar WD scheme. The subbands are generated from each denoised segment. The order of half-band filters is denoted by K_q. Let $C_{Classic-WD}$ is the computational cost of the employed WD process, then it is derivable by considering Fig. 3. At the first stage, two K_q order FIR filters are applied on the $2.N_F$ samples. Onward, the decimation with a factor if 2 is performed. The decimation is performed by selecting up the initial sample, zero index, and then every even indexed sample. Therefore, the arithmetic cost of this operation is minimal. Hence, the computational cost of the first stage of WD is given by Eq. (19).

$$\underbrace{(K_q - 1) \times 2 \times N_F}_{Additions} + \underbrace{K_q \times 2 \times N_F}_{Multiplications} . \quad (19)$$

Roughly N_F and $\frac{N_F}{2}$ samples are respectively processed at the 2nd and 3rd stages of WD by two half-band filters of the K_q order. Four K_q order half-band filters treat the $\frac{N_F}{4}$ samples at the fourth level of WD.

Hence, the overall computational complexity of the WD is given by Eq. (20).

$$C_{FR-WD} = \underbrace{(K_q - 1) \times 4 \times N_F}_{Additions} + \underbrace{K_q \times 4 \times N_F}_{Multiplications} . \quad (20)$$

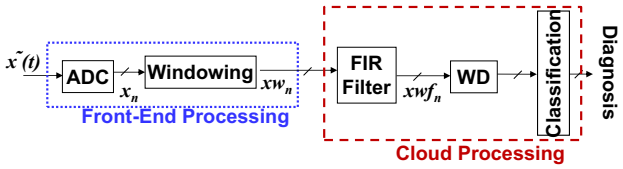

Fig. 4. The block diagram of classical fixed-rate approach.

For the suggested approach, the EASA based segmentation is carried out by performing N^i additions, $2 \times N^i$ comparisons, and N^i increments [34]. Later, the selected segment is resampled by using SLI. It is an additional task which is not required in conventional counterpart. Therefore, the complexity of resampling stage is taken in account for the proposed solution. Nr^i additions and binary weighted right shifts are performed by the *SLI*. The processing costs of right shifts and increments are nominal when compared with additions and multiplications. To compare the complexity of the suggested solution with the fix-rate counterpart, the complexity of a comparison is considered to be the same as that of an addition [45].

Filtering for $W^i$is carried out by using a K=58th order FIR filter, operates at 180Hz. Because of the QRS-complexes selection, the length of segments is 0.5-Seconds. It results in Nr^i=90 samples per segment. In this case K= $0.5K_F$ and Nr^i=$0.28N_F$. Therefore, the computational cost of the filtering operation in the suggested approach is given by Eq. (21).

$$C_{P-FIR} = \underbrace{(0.5 \times K_F - 1) \times (0.28 \times N_F)}_{Additions} + \underbrace{(0.5 \times K_F) \times (0.28 \times N_F)}_{Multiplications}. \quad (21)$$

The filtered signal, xf_n, is decimated with $D = 2$. Therefore, each segment at the WD input contains $M = 0.14 \times N_F$ samples. If K_q is the order of half-band filters, then Eq. (22) presents the arithmetic cost, C_{P-WD}.

$$C_{P-WD} = \underbrace{(K_q - 1) \times 0.56 \times N_F}_{Additions} + \underbrace{K_q \times 0.56 \times N_F}_{Multiplications}. \quad (22)$$

Finally, Eq. (23) and Eq. (24) can be respectively used to compute the overall complexities of the classical and proposed processing chains for each segment.

$$C_{Classic-Total} = \underbrace{(K_F - 1) \times N_F}_{Additions} + \underbrace{K_F \times N_F}_{Multiplications} + \underbrace{(K_q - 1) \times 4 \times N_F}_{Additions} + \underbrace{K_q \times 4 \times N_F}_{Multiplications}. \quad (23)$$

$$C_{P-Total} = \underbrace{(0.5 \times K_F - 1) \times (0.28 \times N_F) + 3 \times N^i + (0.28 \times N_F)}_{Additions} + \underbrace{(K_q - 1) \times 0.56 \times N_F}_{Additions} + \underbrace{(0.5 \times K_F) \times (0.28 \times N_F)}_{Multiplications} + \underbrace{K_q \times 0.56 \times N_F}_{Multiplications}. \quad (24)$$

c) **Fitness Function:** For both considered MOFS algorithms, to evaluate the fitness of solution, the following function, given by Eq. (25), is used [46]:

$$Fitness = \beta E_R + (1 - \beta) \frac{|SEL_f|}{|TOT_f|}. \quad (25)$$

The E_R denotes the classification error, whereas, the number of features selected by a particular FS method is denoted by SEL_f, and TOT_f denotes the total number of features. The parameter β maintains the balance between feature reduction and classification error. In present study, the value of β is fixed at 0.99 [47].

d) **Dimension Reduction Ratio (DRR):** In comparison to t he conventional method, it is a measure of reduction in the amount of data that must be classified. Let P_F and P_b be datasets, have to be processed by classifier respectively in t he traditional and the devised approaches. Then the DDR is given by Eq. (26). Following the work, [17], [9], [41] every element of P_F a n d P_b i s encoded by using 11-Bit resolution. Therefore, the number of bits is not accounte d in Eq. (26).

$$DRR = \frac{P_F}{P_b}. \quad (26)$$

e) **Classification Evaluation Metrics:** The categorization results are assessed using a variety of evaluation tools [48]. These assessments are widely used in the machine learning literature.

TP, TN, FP, and FN stand for true positives, true negatives, false positives, and false negatives, respectively. The following are some of the most often used assessment methods.

$$Acc = \frac{TP+TN}{TP+TN+FP+FN}. \quad (27)$$

$$Sp = \frac{TN}{TN+FP}. \quad (28)$$

$$Se = \frac{TP}{TP+FN}. \quad (29)$$

$$F1 = \frac{2 \times precision \times recall}{precision + recall}. \quad (30)$$

$$kappa = 1 - \frac{1-p_0}{1-p_e}. \quad (31)$$

Where, Acc, Sp, Se and F1 respectively stands for accuracy, specificity, sensitivity and F-measure. In Eq. (30), $precision = \frac{TP}{(TP+FP)}$ and *recall*=Se. In Eq. (31) p_0 is the near-accurate proportion of agreement between the predicted and real labels, and p_e is the theoretical probability of such a correspondence occurring at random, as stated by Eq (32).

$$p_e = \frac{(TP+TN)(TP+FN) + (FP+TN)(FP+FN)}{(TP+TN+FP+FN)^2}. \quad (32)$$

A known two-dimensional graph is the ROC curve [48]. On the X-axis and Y-axis, the "false positive rate" and "true positive rate" are displayed, respectively. The AUC is the area under the ROC curve.

3. Results

The applicability of suggested method is examined for five clinically important categories of arrhythmia [36]. The MATLAB ® is used to implement all ECG signal processing, training, and testing procedures [49]. Simulations are run on a PC with 8GB of RAM and an Intel® Core™ i7-8550U CPU. Examples of windowed heartbeats, classical fix-rate case, for classes PVC and APC are shown in Fig. 5-a and Fig. 5-b respectively. The EASA based segmented versions of these beats are respectively shown in Fig. 5-c and Fig. 5-d. It shows how the sampling densities are concentrated across the QRS complexes while avoiding the acquisition of baseline.

For each class, the average SRR values are calculated for all 450 instances. Each sample is represented with 11-bit resolution in the conventional case [36]. However, the designed LCADC represents each sample as a time-amplitude pair by using 17.4-Bits. This information is used to evaluate the SRR. Summary of findings is outlined in Table 1. Where, STD is abbreviating the standard deviation. The attained average SRR for all 5 classes is 4.04-times. It is accomplished by using an intelligent mix of the LCADC and EASA.

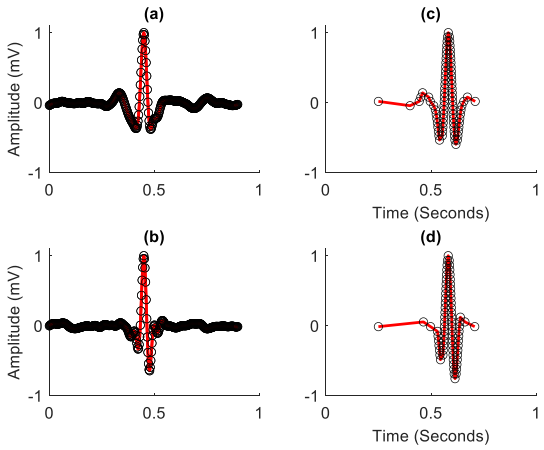

Fig.5. Examples of segmented heart beats (left-column) and selected QRS complexes (right-column).

The selected segments are resampled and then filtered. Each filtered sample is presented with 11-Bit resolution. The filtered segments are decimated with D=2 and are onward decomposed by using the suggested WD scheme. Eqs. (23) and (24) are used to calculate the computational efficiency of the devised processing chain over its fix-rate equivalent. On average, 7.01-times and 7.24-times reduction in the number of additions and multiplications is respectively achieved.

Table 1: Summary of the SRRs for each class.

CLASS	Max	Min	Mean	STD
NS	5.79	3.21	4.29	0.34
PVC	5.78	2.42	4.22	0.50
APC	5.03	2.37	4.06	0.36
LBBB	5.45	2.35	4.09	0.58
RBBB	5.32	1.89	3.56	0.62

In this study, we extracted 36 features per instance using the subbands selection. It renders a features set P_T, of dimension 2250×36. Based on the MPA and ABOA algorithms, features from P_T are extracted. The selection is made by using the Kruskal-Wallis statistical test [50]. The selected features through the said optimization algorithms are then subjected to the Kruskal-Wallis statistical test. The Kruskal-Wallis statistical test has been widely used to confirm the significance and class discrimination ability of feature set. The mentioned statistical test results in the p-values. The features having p-values< 0.05 are considered significant [50], [51], [52], [53]. The selected features through metaheuristic optimization algorithms and their corresponding p-values computed through Kruskal-Wallis statistical test are shown in Table 3. From Table 3, it is evident that all the selected features have the p-values< 0.05,

which confirms their significance [52], [53]. The ✕ in Table 2 indicates that the particular features have not been selected by the corresponding metaheuristic optimization algorithm. It is worth to note here that we have used the metaheuristic search for the whole feature set, which corresponds to the entire dataset.

The selected features and their corresponding p-values are shown in Table 2. The lesser p-values signifies greater ability of the features in classifying the various categories of arrhythmia. After the application of MPA and ABOA, the selected features sets P_1=2250×12 and P_2=2250×16 are respectively obtained. In the traditional fix-rate counterpart the system results in 324 samples per xw_n. By decomposing the xw_n with the similar WD scheme, shown in Fig. 3, results in a features set with a dimension of $P_{Classic}$=2250×355. The DRR of the recommended approach is calculated by using Eq. (26). For the MPA and ABOA algorithms, it respectively results in a 29.59-times and 22.19-times DRR. The convergence plots for the MPA and ABOA algorithms are respectively shown in Fig. 6.

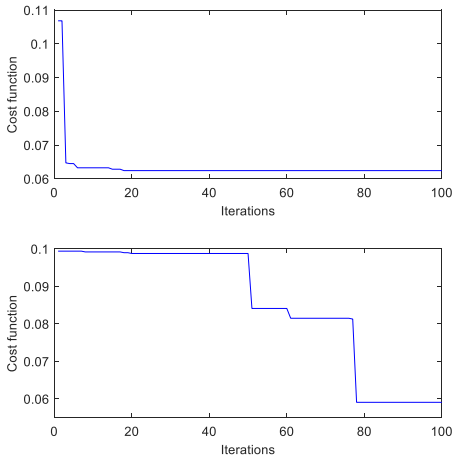

Fig.6. The convergence plots: For the MPA (top-row) and for the BOA (bottom-row).

The classification results obtained for P_R are compared to those obtained for the P_T, P_1 and P_2. It illustrate the benefit of using the frequency content based subbands selection and MOFS techniques. All results are detailed in Tables 3-5. These exhibit all evaluation measures for the considered classifiers. All assessment measures demonstrate that all studied classifiers perform well.

Table 2: The Map of Selected Features

Feature number	Features (P_T)	p-values of selected features using various FS algorithms	
		MPA	ABOA
1	$aa4_1$	✕	✕
2	$aa4_2$	✕	✕
3	$aa4_3$	✕	✕
4	$aa4_4$	✕	✕
5	$aa4_5$	6.18E-21	6.14E-21
6	$aa4_6$	✕	2.61E-135
7	$aa4_7$	✕	2.39E-200
8	$aa4_8$	6.6E-154	✕
9	$aa4_9$	✕	9.60E-179
10	$aa4_{10}$	✕	1.84E-121
11	$ad4_1$	✕	✕
12	$ad4_2$	✕	✕
13	$ad4_3$	✕	✕
14	$ad4_4$	2.87E-06	2.87E-06
15	$ad4_5$	✕	4.44E-140
16	$ad4_6$	8.3E-140	✕
17	$ad4_7$	✕	3.68E-128
18	$ad4_8$	✕	✕
19	$ad4_9$	2E-282	✕
20	$ad4_{10}$	4.3E-111	4.25E-111
21	$da4_1$	✕	3.67E-101
22	$da4_2$	✕	✕
23	$da4_3$	✕	✕
24	$da4_4$	0.000238	✕
25	$da4_5$	✕	✕
26	$da4_6$	4.63E-66	✕
27	$da4_7$	✕	✕
28	$da4_8$	✕	✕
29	$da4_9$	✕	✕
30	$da4_{10}$	✕	9.41E-109
31	$dd4_1$	✕	8.50E-129
32	$dd4_2$	✕	✕
33	$dd4_3$	1.86E-43	✕
34	$dd4_4$	9.4E-109	2.318E-62
35	$dd4_5$	4.8E-287	4.81E-287
36	$dd4_6$	✕	✕
37	$dd4_7$	✕	✕
38	$dd4_8$	✕	2.22E-182
39	$dd4_9$	✕	8.55E-197
40	$dd4_{10}$	8.3E-289	✕

Table 3 shows that for P_R, P_1 and P_2 the highest accuracies of respectively 98.83%, 98.38% and 98.86% are secured by the RF. For P_T the highest accuracy of 98.83% is attained by the ANN. For P_T the accuracy of RF is 0.06% lower than ANN. The highest specificities of 99.26%, 98.98% and 99.29% are also achieved by RF for P_R, P_1 and P_2 respectively. The ANN secures the highest specificity of 99.27% for P_T. The specificity of RF is 0.04% lower than ANN for the case of P_T.

Table 3: The Accuracy and Specificity of different classifiers

	Acc (%age)				Sp (%age)			
Classifier/ Dataset	P_R	P_T	P_1	P_2	P_R	P_T	P_1	P_2
ANN	98.59	**98.83**	97.96	98.50	99.12	**99.27**	98.72	99.06
KNN	98.64	98.49	97.96	98.57	99.15	99.06	98.72	99.11
SVM	98.33	97.71	96.12	97.64	98.96	98.57	97.55	98.52
RF	**98.83**	98.77	**98.38**	**98.86**	**99.26**	99.23	**98.98**	**99.29**

Table 4 presents that for P_R, P_1 and P_2 the highest F1 values of respectively 97.12%, 96.04% and 97.20% are secured by the RF. For P_T the highest F1 value of 97.11% is attained by the ANN. For P_T the F1 value of RF is the second highest and it is 0.13% lesser than ANN. The Kappa values of 98.51%, 97.93% and 98.56% are also achieved by RF for P_R, P_1 and P_2 respectively. The ANN secures the

highest Kappa value of 98.51% for P_T. The Kappa value of RF is the second highest and it is 0.07% lesser than ANN for the case of P_T.

Table 4: The F-measure and Kappa values of different classifiers

	F1 (%age)				Kappa (%age)			
Classifier/ Dataset	P_R	P_T	P_1	P_2	P_R	P_T	P_1	P_2
ANN	96.54	**97.11**	95.02	96.31	98.21	**98.51**	97.38	98.09
KNN	96.68	96.32	95.04	96.50	98.28	98.09	97.38	98.18
SVM	95.92	94.47	90.83	94.29	97.87	97.06	94.92	96.96
RF	**97.12**	96.98	**96.04**	**97.20**	**98.51**	98.44	**97.93**	**98.56**

Table 5 displays that for P_R, P_1 and P_2 the highest sensitivities of respectively 97.11%, 96.04% and 97.20% are secured by the RF. For P_T the highest sensitivity of 97.14% is achieved by the ANN. For P_T the RF follows ANN with 0.16% lower sensitivity. The highest AUC values of 99.86%, 99.86%, 99.80% and 99.86% are reached by RF for P_R, P_T, P_1 and P_2 respectively.

Table 5: The Sensitivity and AUC results of different classifiers

	Se (%age)				AUC (%age)			
Classifier/ Dataset	P_R	P_T	P_1	P_2	P_R	P_T	P_1	P_2
ANN	96.53	**97.14**	95.02	96.31	99.18	99.06	98.78	99.06
KNN	96.67	96.31	95.02	96.49	99.32	99.24	99.02	99.26
SVM	95.91	94.44	90.79	94.27	98.56	98.26	97.10	98.20
RF	**97.11**	96.98	**96.04**	**97.20**	**99.86**	**99.86**	**99.80**	**99.86**

Tables 3-5 confirm a superior performance of the RF compared to the ANN, KNN and SVM for most of the intended cases, P_R, P_T, P_1 and P_2. the highest scores are attained for P_2 by the RF classifier. The confusion matrices, obtained with RF for the P_R, P_T, P_1 and P_2, are respectively presented in Tables 6-9.

Table 6: The confusion matrix for the case of P_R (RF classifier)

P_R		Predicted				
		NS	APC	LBBB	PVC	RBBB
Actual	NS	436	0	7	2	5
	APC	2	442	1	3	2
	LBBB	29	0	419	0	2
	PVC	2	0	0	442	6
	RBBB	2	1	0	1	446

Table 7: The confusion matrix for the case of P_T (RF classifier)

P_T		Predicted				
		NS	APC	LBBB	PVC	RBBB
Actual	NS	433	1	11	2	3
	APC	3	441	1	3	2
	LBBB	21	3	426	0	0
	PVC	3	4	3	436	4
	RBBB	1	3	0	0	446

Table 8: The confusion matrix for the case of P_1 (RF classifier)

P_1		Predicted				
		NS	APC	LBBB	PVC	RBBB
Actual	NS	428	1	15	2	3
	APC	2	440	1	3	4
	LBBB	28	2	416	2	2
	PVC	5	1	2	436	6
	RBBB	2	5	1	2	440

Table 9: The confusion matrix for the case of P_2 (RF classifier)

P_2		Predicted				
		NS	APC	LBBB	PVC	RBBB
Actual	NS	443	0	11	2	2
	APC	2	443	2	2	1
	LBBB	22	1	424	0	3
	PVC	4	1	0	441	4
	RBBB	2	3	0	1	444

4. Discussion

The front-end module of the suggested system works at adaptive-rate, accomplished by using the LCADC. Moreover, the EASA segments the QRS complexes. The effective online adjustment of Fs^i with QRS selection prevents the collection of unneeded information and improves the SRR. On average a 4.04-times SRR is obtained for the studied case. It also aptitudes a decrease in wireless data transmitter activity.

The cloud-side modules also get benefit of the multirate processing, accomplished by efficiently introducing a lower-tap filter and decimation stage prior to the WD. It induces a reduction in the cloud processing load while performing the resampling, filtering and WD. For the studied case, the average gains of 7.01-times and 7.24-times, in terms of additions and multiplications are respectively achieved. Additionally, the suggested method attains the 29.59-times and 22.19-times DRR respectively for the MPA and ABOA. It promises a considerable decrease in the processing cost and latency of the classification stage.

The MPA and ABOA based features selection of the selected subband reduces the dataset dimension significantly. However the system might lag in the classification performance when compared to the case of P_R. Consequently, the performance is evaluated for multiple settings namely P_R, P_T, P_1 and P_2. The RF has the best performance of all the classifiers tested, with a score of 98.86% accuracy for P_2. The highest accuracies for the case of P_R, P_T and P_1 are respectively 0.03%, 0.03% and 0.48% lower than the one obtained for P_2. It assures the efficacy of suggested MO based features selection from chosen subbands.

While considering all settings, P_R, P_T, P_1 and P_2, the highest scores are attained for P_2 by RF. These are 99.29%, 97.20%, 98.56%, 97.20% and 99.86% scores respectively for Sp, F1, Kappa, Se and AUC. It shows that being an ensemble classifier the RF attains the least biasness when compared with KNN, SVM and ANN.

The MPA outperforms the ABOA in terms of DRR. However, the highest accuracy scores, achieved for the MPA, are a bit less than the ones obtained for the ABOA. It shows a tradeoff between the arrhythmia identification accuracy with DRR. A suitable choice can be made after consulting with medical practitioners.

A 4.4-Bit resolution LCADC is used in the suggested approach. In the counterparts, based on fix-rate uniform sampling, an ADC with 11-bit resolution is used for digitization [7],[10],[11]-[15],[36]. It indicates that a simpler circuit level implementation might be realized in the case of devised approach. In the conventional tactic, a reduction in M will diminish the SNR of ADC [38]. It can decline the

classification accuracy. However, the effective resolution of LCADC is independent of M [38]. Therefore, even with a 4.4-bit resolution, the suggested method achieves an accuracy of 98.86%.

The advantages of our approach are a high precision automated arrhythmia recognition with noticeable SRR, DRR and computational effectiveness. It makes the devised method attractive and useful for designing the efficient mobile solutions for the ECG based automated cardiac health monitoring. The potential uses are the cardiac patients monitoring in remote areas and emergency notification of cardiac arrest.

The results of key prior studies, utilizing the same ECG dataset are compared with the proposed approach. Table 10 summarizes and compares the highest identification accuracies for all considered studies. It assures that the proposed solution achieves a comparable performance.

Table 10 shows that a high accuracy is also attained with counter fix-rate solutions [10], [13], [18]. However, in these studies the entire signal is acquired and transmitted to cloud at a fix-rate regardless of the signal content. On cloud the received information is processed by using the deep learning approaches. Compared to the suggested approach it causes an increased transmission activity and power consumption of the battery operated wireless ECG wearables. Moreover, the usage of deep learning can also results in an augmented computational cost on the cloud side compared to the proposed method. Consequently, these methods, [10], [13], [18], are not the best suited for mobile healthcare.

Table 10: Comparison with State-of-the-Art Solutions

Study	Classifier	Pre Condition.	Feature Extraction	Classes	Acc. (%)
[7]	DNN	Digital Filtering	LSTM based DLM and GA	5	98.00
[10]	LSTM	Segmentation	Nonlinear Encoding Structure	5	99.00
[12]	CNN	Digital Filtering	No	5	94.03
[13]	2-D CNN	Segmentation	Spectrogram	5	99.00
[15]	CNN+ LSTM	Segmentation + Z-score normalization	No	5	98.10
[17]	RF	Digital Filtering	DWT+ Subbands Statistical Features + MI based FS	5	97.00
[18]	SVM	Segmentation	LSTM based Auto Encoder	5	99.45
[19]	RF	Adaptive Rate Digital Filtering	DWT	5	97.00
This Study	**RF**	**Digital Filtering**	**WD + Subbands Selection + MO based FS**	**5, (P_1)**	**98.38**
				5, (P_2)	**98.86**

5. Conclusion

An original ECG processing based automated arrhythmia diagnosis approach is devised. It employs a novel mix of the level-crossing ADCs, enhanced activity selection, multirate processing, wavelet decomposition, subbands selection, metaheuristic optimization based features selection, and machine learning algorithms. Results have demonstrated that this method focuses on the QRS complexes while ignoring the redundant baseline. This significantly decreases the volume of data to be transmitted and processed on cloud when compared with fixed-rate alternatives. The overall samples reduction ratio of 4.04-times is attained by the front-end processing module. The total average computational gains of 7.01-times and 7.24-times, in terms of additions and multiplications, are secured by the cloud based conditioning and wavelet decomposition stages. Moreover, the system attains 29.59-times and 22.19-times dimension reduction ratios respectively for the MPA and ABOA. The highest classification accuracies of 98.38% and 98.86% are obtained respectively for the MPA and ABOA. This performance is comparable with the existing contemporary approaches. It confirms the potential of suggested approach in terms of compression and computing efficacy without losing the accuracy. The performance of proposed solution is tested for the multi-subjects and multi-class MIT-BIH dataset. However, a limitation of this study is the consideration of a particular number of MIT-BIH dataset records. In future the performance will be studied for most of the related MIT-BIH dataset records and while considering the extended categories of arrhythmia. The subject based testing will also be performed. Furthermore, the performance of devised method will also be evaluated for other potential biomedical datasets and applications. Moreover, incorporation of deep learning algorithms can improve the system accuracy but at an increased computational cost. Investigating this feasibility is another prospect.

Acknowledgement: The project is funded by the Effat University, under the grant number UC#9/29 April.2020/7.1-22(2)1.

Data Availability: The dataset used in this paper is public ly available at: https://physionet.org/content/mitdb/1.0.0/

Conflicts of Interest: Authors declare no conflict of interest.

Ethical approval: This article does not contain any studies with human participants or animals performed by any of the authors.

References

[1] E. J. Benjamin *et al.*, "Heart disease and stroke Statistics-2019 update a report from the American Heart Association," *Circulation*, 2019.

[2] S. Banerjee and M. Mitra, "Application of cross wavelet transform for ECG pattern analysis and classification," *IEEE*

Trans. Instrum. Meas., vol. 63, no. 2, pp. 326–333, 2013.
[3] S. Raj and K. C. Ray, "ECG signal analysis using DCT-based DOST and PSO optimized SVM," *IEEE Trans. Instrum. Meas.*, vol. 66, no. 3, pp. 470–478, 2017.
[4] F. Tueche, Y. Mohamadou, A. Djeukam, L. C. N. Kouekeu, R. Seujip, and M. Tonka, "Embedded Algorithm for QRS Detection Based on Signal Shape," *IEEE Trans. Instrum. Meas.*, vol. 70, pp. 1–12, 2021.
[5] A. Josko and R. J. Rak, "Effective simulation of signals for testing ECG analyzer," *IEEE Trans. Instrum. Meas.*, vol. 54, no. 3, pp. 1019–1024, 2005.
[6] E. Keenan, C. Karmakar, F. C. Brownfoot, and M. Palaniswami, "Personalized Anatomic Modeling for Noninvasive Fetal ECG: Methodology and Applications," *IEEE Trans. Instrum. Meas.*, vol. 70, pp. 1–12, 2021.
[7] M. Hammad, A. M. Iliyasu, A. Subasi, E. S. Ho, and A. A. Abd El-Latif, "A multitier deep learning model for arrhythmia detection," *IEEE Trans. Instrum. Meas.*, vol. 70, pp. 1–9, 2020.
[8] S. M. Qaisar and D. Dallet, "ECG Noise Removal and Efficient Arrhythmia Identification Based on Effective Signal-Piloted Processing and Machine Learning," 2021, pp. 1–6.
[9] S. Sahoo, B. Kanungo, S. Behera, and S. Sabut, "Multiresolution wavelet transform based feature extraction and ECG classification to detect cardiac abnormalities," *Measurement*, vol. 108, pp. 55–66, 2017.
[10] O. Yildirim, U. B. Baloglu, R.-S. Tan, E. J. Ciaccio, and U. R. Acharya, "A new approach for arrhythmia classification using deep coded features and LSTM networks," *Comput. Methods Programs Biomed.*, vol. 176, pp. 121–133, 2019.
[11] D. K. Atal and M. Singh, "Arrhythmia Classification with ECG signals based on the Optimization-Enabled Deep Convolutional Neural Network," *Comput. Methods Programs Biomed.*, vol. 196, p. 105607, 2020.
[12] U. R. Acharya *et al.*, "A deep convolutional neural network model to classify heartbeats," *Comput. Biol. Med.*, vol. 89, pp. 389–396, 2017.
[13] J. Huang, B. Chen, B. Yao, and W. He, "ECG arrhythmia classification using STFT-based spectrogram and convolutional neural network," *IEEE Access*, vol. 7, pp. 92871–92880, 2019.
[14] M. M. Al Rahhal, Y. Bazi, H. AlHichri, N. Alajlan, F. Melgani, and R. R. Yager, "Deep learning approach for active classification of electrocardiogram signals," *Inf. Sci.*, vol. 345, pp. 340–354, 2016.
[15] S. L. Oh, E. Y. Ng, R. San Tan, and U. R. Acharya, "Automated diagnosis of arrhythmia using combination of CNN and LSTM techniques with variable length heart beats," *Comput. Biol. Med.*, vol. 102, pp. 278–287, 2018.
[16] Ö. Yıldırım, P. Pławiak, R.-S. Tan, and U. R. Acharya, "Arrhythmia detection using deep convolutional neural network with long duration ECG signals," *Comput. Biol. Med.*, vol. 102, pp. 411–420, 2018.
[17] S. M. Qaisar and S. F. Hussain, "An effective arrhythmia classification via ECG signal subsampling and mutual information based subbands statistical features selection," *J. Ambient Intell. Humaniz. Comput.*, pp. 1–15, 2021.
[18] B. Hou, J. Yang, P. Wang, and R. Yan, "LSTM-based auto-encoder model for ECG arrhythmias classification," *IEEE Trans. Instrum. Meas.*, vol. 69, no. 4, pp. 1232–1240, 2019.
[19] S. Mian Qaisar and S. Fawad Hussain, "Arrhythmia Diagnosis by Using Level-Crossing ECG Sampling and Sub-Bands Features Extraction for Mobile Healthcare," *Sensors*, vol. 20, no. 8, p. 2252, 2020.
[20] S. Majumder, L. Chen, O. Marinov, C.-H. Chen, T. Mondal, and M. J. Deen, "Noncontact wearable wireless ECG systems for long-term monitoring," *IEEE Rev. Biomed. Eng.*, vol. 11, pp. 306–321, 2018.
[21] C. J. Deepu, X. Zhang, C. H. Heng, and Y. Lian, "A 3-lead ECG-on-chip with QRS detection and lossless compression for wireless sensors," *IEEE Trans. Circuits Syst. II Express Briefs*, vol. 63, no. 12, pp. 1151–1155, 2016.
[22] Z. Chen *et al.*, "An energy-efficient ECG processor with weak-strong hybrid classifier for arrhythmia detection," *IEEE Trans. Circuits Syst. II Express Briefs*, vol. 65, no. 7, pp. 948–952, 2017.
[23] N. Ravanshad, H. Rezaee-Dehsorkh, R. Lotfi, and Y. Lian, "A level-crossing based QRS-detection algorithm for wearable ECG sensors," *IEEE J. Biomed. Health Inform.*, vol. 18, no. 1, pp. 183–192, 2013.
[24] T. Marisa *et al.*, "Pseudo asynchronous level crossing ADC for ECG signal acquisition," *IEEE Trans. Biomed. Circuits Syst.*, vol. 11, no. 2, pp. 267–278, 2017.
[25] T. Tekeste, H. Saleh, B. Mohammad, and M. Ismail, "Ultra-low power QRS detection and ECG compression architecture for IoT healthcare devices," *IEEE Trans. Circuits Syst. Regul. Pap.*, vol. 66, no. 2, pp. 669–679, 2018.
[26] V. Mazaheri and H. Khodadadi, "Heart arrhythmia diagnosis based on the combination of morphological, frequency and nonlinear features of ECG signals and metaheuristic feature selection algorithm," *Expert Syst. Appl.*, vol. 161, p. 113697, 2020.
[27] M. Abdelazez, S. Rajan, and A. D. Chan, "Detection of atrial fibrillation in compressively sensed electrocardiogram measurements," *IEEE Trans. Instrum. Meas.*, vol. 70, pp. 1–9, 2020.
[28] Z. Yang, Q. Zhou, L. Lei, K. Zheng, and W. Xiang, "An IoT-cloud based wearable ECG monitoring system for smart healthcare," *J. Med. Syst.*, vol. 40, no. 12, p. 286, 2016.
[29] Y. Jiang *et al.*, "EventDTW: An Improved Dynamic Time Warping Algorithm for Aligning Biomedical Signals of Nonuniform Sampling Frequencies," *Sensors*, vol. 20, no. 9, p. 2700, 2020.
[30] D. Mitra, H. Zanddizari, and S. Rajan, "Investigation of kronecker-based recovery of compressed ecg signal," *IEEE Trans. Instrum. Meas.*, vol. 69, no. 6, pp. 3642–3653, 2019.
[31] J. Zhang, Z. L. Yu, Z. Gu, Y. Li, and Z. Lin, "Multichannel Electrocardiogram Reconstruction in Wireless Body Sensor Networks Through Weighted $\ell_ {1, 2} $ Minimization," *IEEE Trans. Instrum. Meas.*, vol. 67, no. 9, pp. 2024–2034, 2018.
[32] K. N. Pandagre, "Detection of Arrhythmia Disease in Ecg Signal Using Optimal Features," *Int. J. Inf. Technol. IJIT*, vol. 6, no. 5, 2020.
[33] E. H. Houssein, I. E. Ibrahim, N. Neggaz, M. Hassaballah, and Y. M. Wazery, "An efficient ECG arrhythmia classification method based on Manta ray foraging optimization," *Expert Syst. Appl.*, vol. 181, p. 115131, 2021.
[34] S. M. Qaisar, "Efficient mobile systems based on adaptive rate signal processing," *Comput. Electr. Eng.*, vol. 79, p. 106462, 2019.
[35] S. M. Qaisar and L. Fesquet, "An Effective QRS Selection Based on the Level-Crossing Sampling and Activity Selection," 2020, pp. 1–5.
[36] G. B. Moody and R. G. Mark, "The impact of the MIT-BIH arrhythmia database," *IEEE Eng. Med. Biol. Mag.*, vol. 20, no. 3, pp. 45–50, 2001.
[37] A. Antoniou, *Digital signal processing*. McGraw-Hill, 2016.
[38] S. Mian Qaisar, "Échantillonnage et traitement conditionnés par le signal: une approche prometteuse pour des traitements efficaces à pas adaptatifs," 2009.

[39] S. M. Qaisar, M. Akbar, T. Beyrouthy, W. Al-Habib, and M. Asmatulah, "An error measurement for resampled level crossing signal," 2016, pp. 1–4.
[40] S. M. Anwar, M. Gul, M. Majid, and M. Alnowami, "Arrhythmia classification of ECG signals using hybrid features," *Comput. Math. Methods Med.*, vol. 2018, 2018.
[41] T. Li and M. Zhou, "ECG classification using wavelet packet entropy and random forests," *Entropy*, vol. 18, no. 8, p. 285, 2016.
[42] A. Faramarzi, M. Heidarinejad, S. Mirjalili, and A. H. Gandomi, "Marine Predators Algorithm: A nature-inspired metaheuristic," *Expert Syst. Appl.*, vol. 152, p. 113377, 2020.
[43] X. Qi, Y. Zhu, and H. Zhang, "A new meta-heuristic butterfly-inspired algorithm," *J. Comput. Sci.*, vol. 23, pp. 226–239, Nov. 2017, doi: 10.1016/j.jocs.2017.06.003.
[44] A. Subasi, *Practical guide for biomedical signals analysis using machine learning techniques: A MATLAB based approach*. Academic Press, 2019.
[45] I. Koren, *Computer arithmetic algorithms*. CRC Press, 2018.
[46] E. Emary, H. M. Zawbaa, and A. E. Hassanien, "Binary grey wolf optimization approaches for feature selection," *Neurocomputing*, vol. 172, pp. 371–381, 2016.
[47] J. Too, A. R. Abdullah, N. Mohd Saad, and N. Mohd Ali, "Feature selection based on binary tree growth algorithm for the classification of myoelectric Signals," *Machines*, vol. 6, no. 4, p. 65, 2018.
[48] C. M. Bishop, *Pattern recognition and machine learning*. springer, 2006.
[49] H. Klee and R. Allen, *Simulation of dynamic systems with MATLAB® and Simulink®*. Crc Press, 2018.
[50] Y. Chan and R. P. Walmsley, "Learning and understanding the Kruskal-Wallis one-way analysis-of-variance-by-ranks test for differences among three or more independent groups," *Phys. Ther.*, vol. 77, no. 12, pp. 1755–1761, 1997.
[51] L. Kennedy-Shaffer, "Before p< 0.05 to beyond p< 0.05: using history to contextualize p-values and significance testing," *Am. Stat.*, vol. 73, no. sup1, pp. 82–90, 2019.
[52] S. I. Khan, S. M. Qaisar, and R. B. Pachori, "Automated classification of valvular heart diseases using FBSE-EWT and PSR based geometrical features," *Biomed. Signal Process. Control*, vol. 73, p. 103445, 2022.
[53] F. Massa *et al.*, "Utility of quantitative EEG in early Lewy body disease," *Parkinsonism Relat. Disord.*, vol. 75, pp. 70–75, 2020.